Supplementary Material: Hierarchical Ni/Co-based oxynitride nanoarrays with superior lithiophilicity for high-performance lithium metal anode

MAIN TEXT (optional)

SEM images and XRD pattern of bare Ni foam, SEM images of Ni-Co precursor, the corresponding elemental maps of the obtained NiCoON/NF, SEM images, XRD pattern and the corresponding elemental maps of NiCoO/NF, the low-magnification TEM image and high-resolution TEM image of NiCoO/NF, BET characterization of the NiCoON, the XPS spectra of survey spectra of NiCoON/NF and NiCoO/NF, Coulombic efficiencies of NF, NiCoO/NF and NiCoON/NF, XRD patterns and the corresponding elemental maps of Li@NiCoON/NF after deposition of Li, Comparison of CE performance and voltage hysteresis of NiCoON/NF obtained from previsouly-reported different 3D hosts.

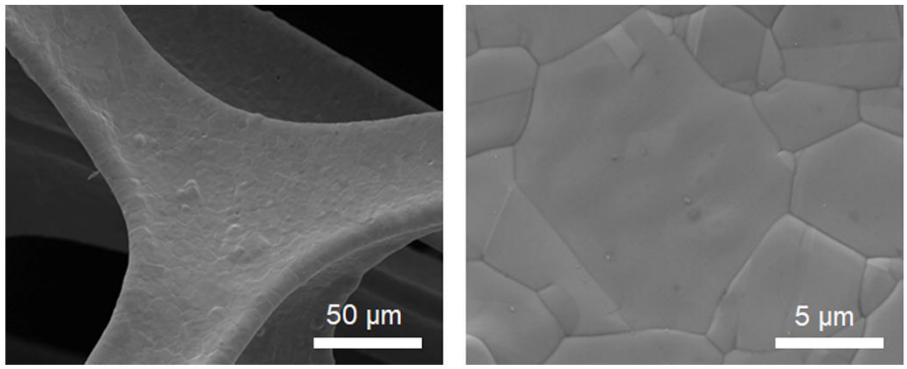

Supplementary Figure 1. SEM images of bare Ni foam.

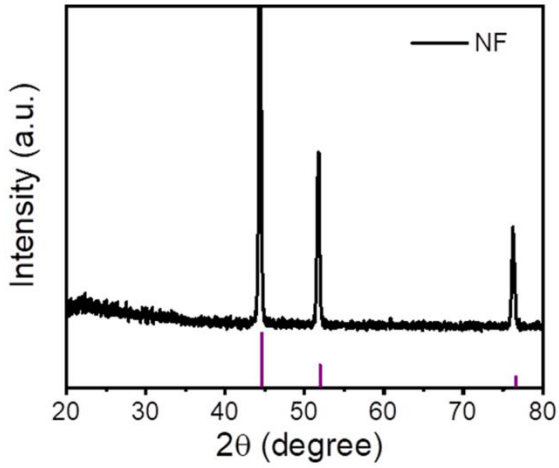

Supplementary Figure 2. XRD pattern of bare Ni foam.

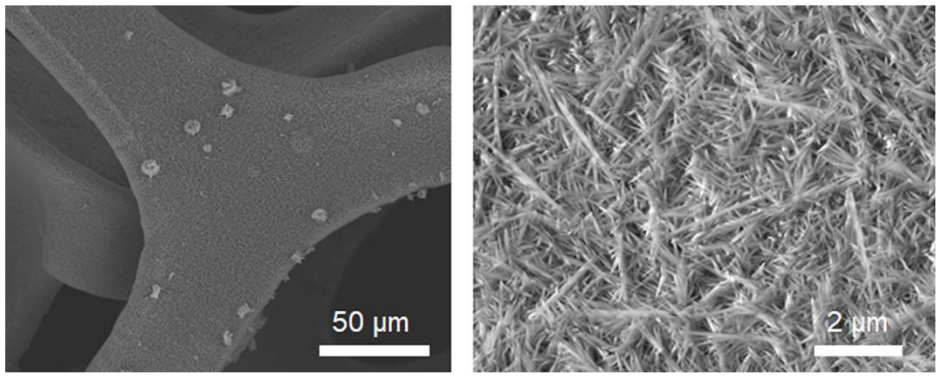

Supplementary Figure 3. SEM images of Ni-Co precursor.

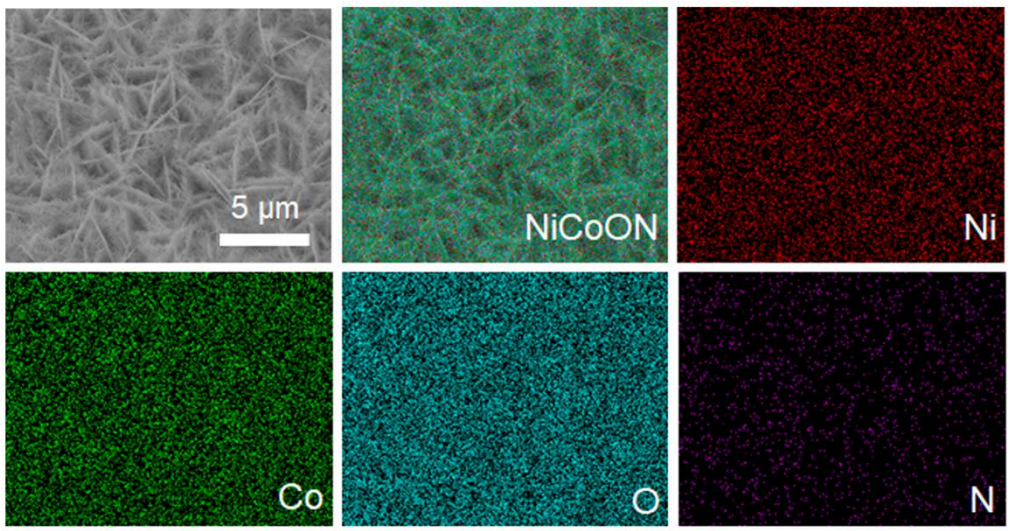

Supplementary Figure 4. The corresponding elemental maps of NiCoON/NF.

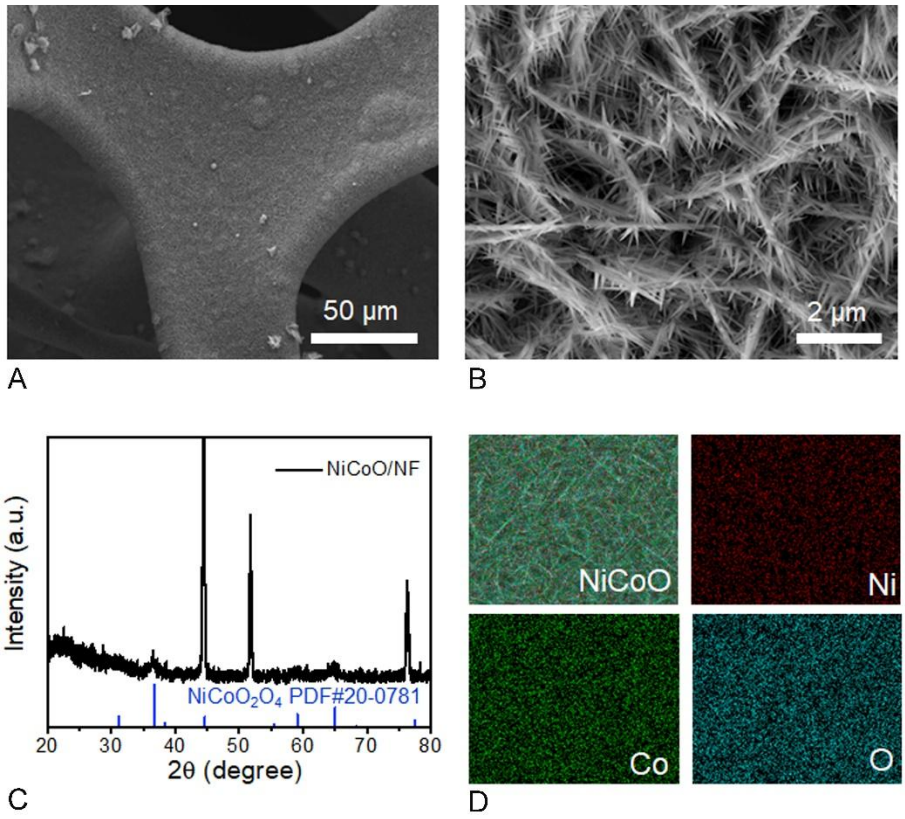

Supplementary Figure 5. (A, B): SEM images of NiCoO/NF; (C): XRD pattern of NiCoO/NF; (D): The corresponding elemental maps of NiCoO/NF.

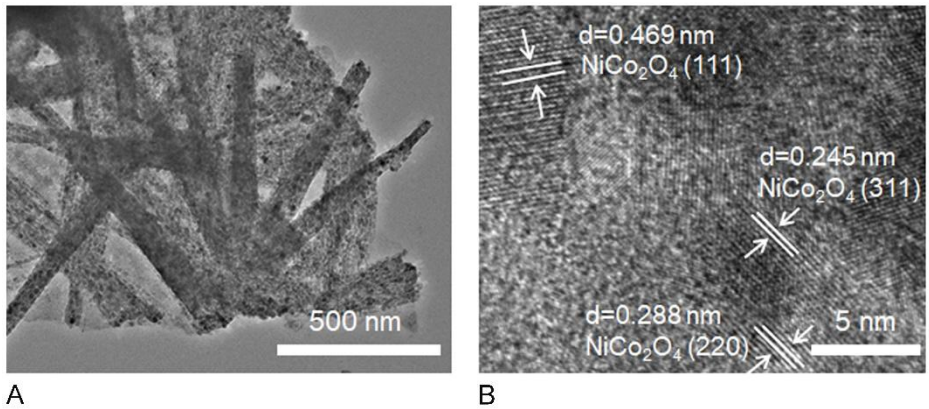

Supplementary Figure 6. (A): The low-magnification TEM image and (B): high-resolution TEM image of NiCoO/NF.

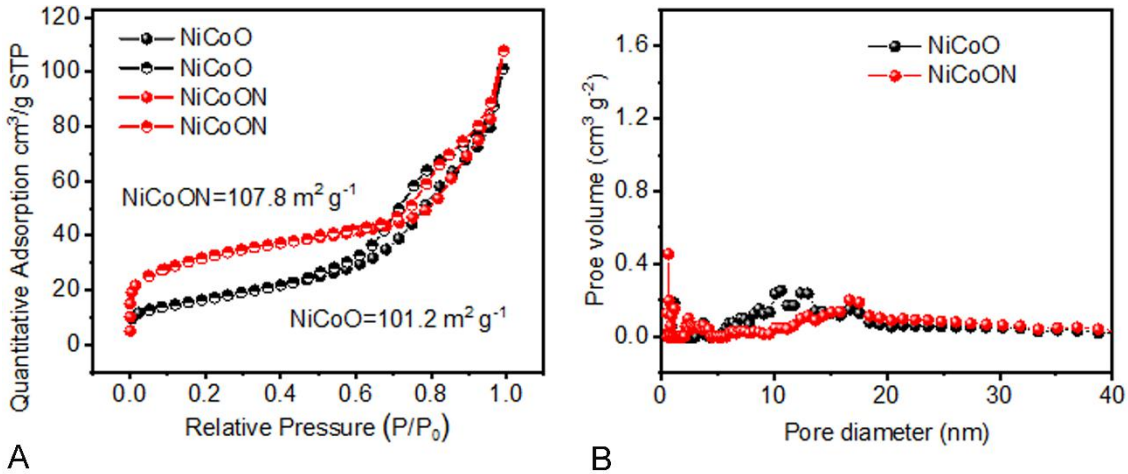

Supplementary Figure 7. (A): BET characterization and (B): Nitrogen adsorption–desorption isotherms and pore size distribution plots of the NiCoON.

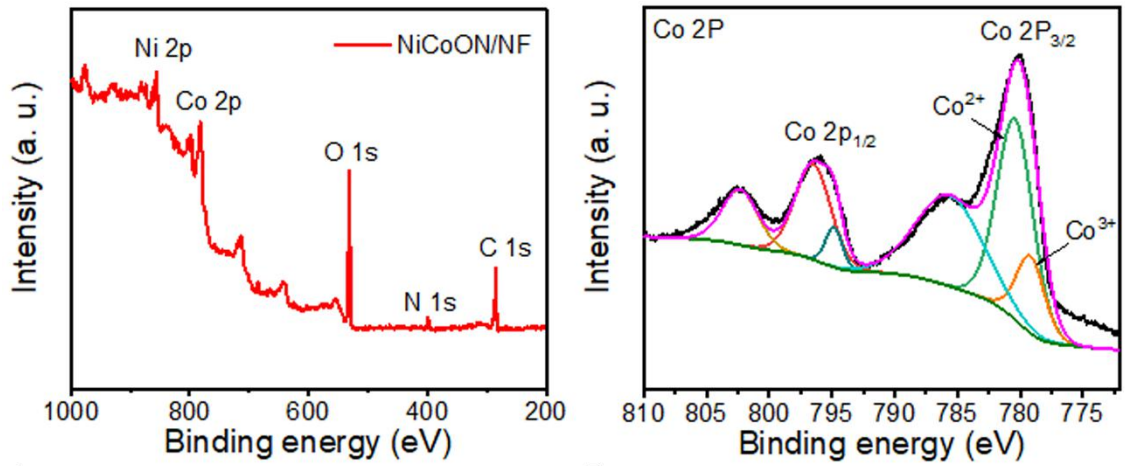

Supplementary Figure 8. (A): The XPS spectra of survey spectra of NiCoON/NF; (B) Co 2p XPS spectra of NiCoON/NF.

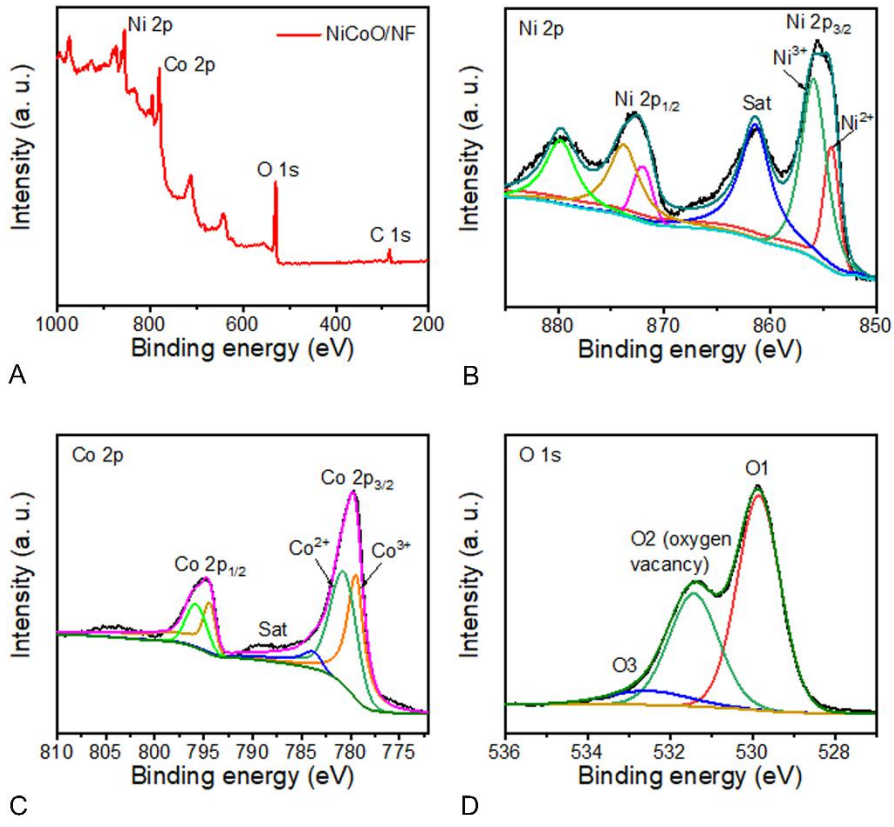

Supplementary Figure 9. (A) The XPS spectra of survey spectra of NiCoO/NF, high resolution XPS spectra of (B) Ni 2p, (C) Co 2p and (D) O 1s.

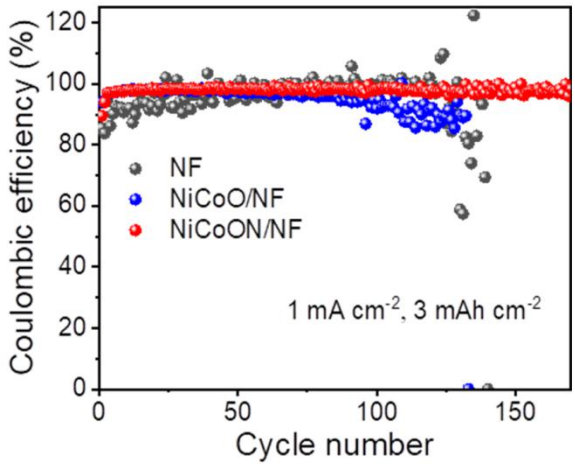

Supplementary Figure 10. The Coulombic efficiencies of NF, NiCoO/NF and NiCoON/NF at 1 mA cm^{-2} with the plating capacity of 3 mAh cm^{-2}.

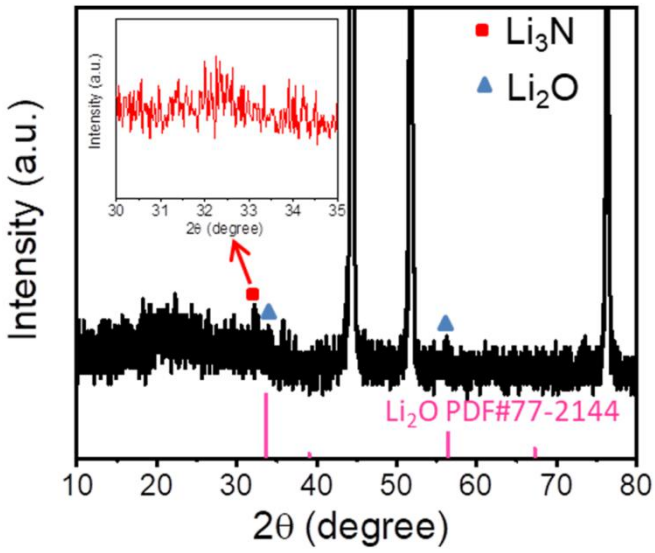

Supplementary Figure 11. XRD patterns of Li@NiCoON/NF with 1 mAh cm^{-2} of Li.

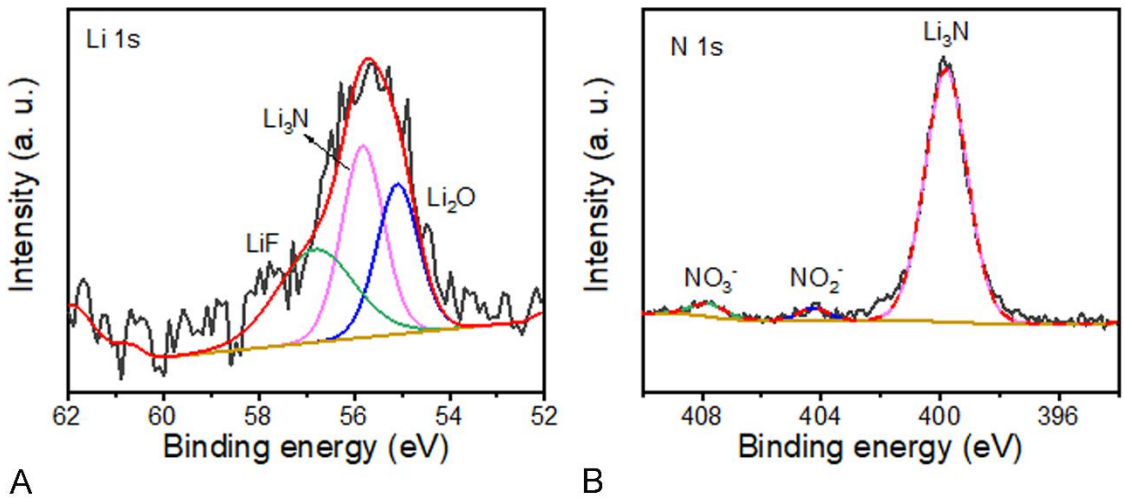

Supplementary Figure 12. XPS spectra of (A) Li 1 s and (B) N 1 s of the Li@NiCoON/NF with 1 mAh cm^{-2} of Li.

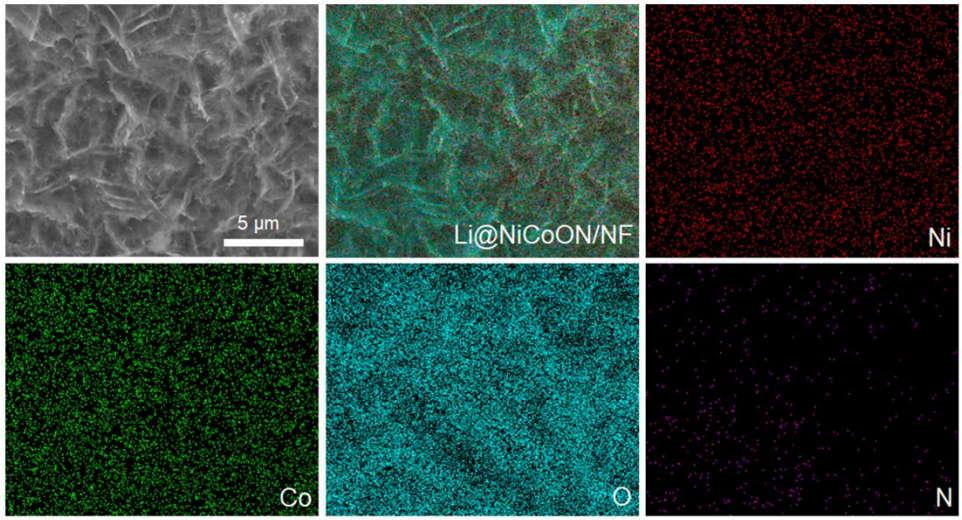

Supplementary Figure 13. SEM images of NiCoON/NF after plating 1 mAh cm^{-2} of Li and the corresponding elemental maps of Ni, Co, O, and N.

Supplementary Table 1. Comparison of CE performance of NiCoON/NF obtained from previsouly-reported different 3D hosts.

Electrode materials	Current density (mA cm^{-2})	Capacity (mAh cm^{-2})	Cycling number	Coulombic efficiency (%)
CuON/CF[1]	0.5	1	450	98.8
	2	1	100	> 98
Cu_2S nanowires inside the Cu foam[2]	1	1	150	> 95.5
	2	1	150	> 95.5
Double metal oxides on Cu foil[3]	0.5	1	230	98
	1	1	180	94
Ni_3N modified Ni foam[4]	1	1	300	97
Co_3N/NF[5]	0.5	1	200	98.3
	1	1	120	96.9
NiO plates decorated Ni collector[6]	1	1	140	97

$NiCo_2O_4$ nanorods anchored on Ni foam[7]	1	1	500	98.7
NiF_x nanosheets on Ni foam[8]	1	1	450	97.1
Cu fibers on the Cu foam[9]	1	1	200	98
N-doped CNTs on Ni foam[10]	1	1	200	98.2
	2	1	100	98
Cu-CuO-Ni[11]	1	1	250	95
Graphene network nested Cu foam[12]	1	1	200	98
CuO NAs/CF[13]	0.5	1	200	97
	1	1	180	98
This work	1	1	600	98.4
	2	1	400	97.3
	5	1	120	97.2
	2	2	200	97.1

Supplementary Table 2. Comparison of voltage hysteresis of NiCoON/NF obtained from previsouly-reported different 3D current collectors.

Electrode materials	**Current density (mA cm^{-2})**	**Capacity (mAh cm^{-2})**	**Cycling time (h)**	**Voltage hysteresis (mV)**
Ni_3N modified Ni foam[4]	1	1	400	13
	5	1	160	39
Co_3N/NF[5]	1	1	1200	22
$NiCo_2O_4$ nanorods anchored on Ni	1	1	1000	16

foam[7]				
NiF_x nanosheets on Ni foam[8]	1	3	600	80
Cu fibers on the Cu foam[9]	1	1	800	25
N-doped CNTs on Ni foam[10]	1	1	1000	29
Cu-CuO-Ni[11]	0.5	0.5	580	~59
Graphene network nested Cu foam[12]	1 2	1 1	1300 500	~30 50
CuO NAs/CF[13]	0.5	0.5	600	30
VA-CuO-Cu[14]	0.2 0.5	0.5 0.5	1500 700	20 25
Graphene anchored on Cu foam[15]	0.5	1	2000	10
Plasma-Strengthened CuO Nanosheet on Cu foil[16]	1	1	600	23.1
vertically aligned Cu with microchannels[17]	1 2	1 2	200 100	20 50
This work	1 5 1	1 1 3	1000 150 2000	24 65 20

REFERENCES

1. Lei MN, You ZY, Ren LB, Liu XR, Wang JG. Construction of copper oxynitride nanoarrays with enhanced lithiophilicity toward stable lithium metal anodes. *J Power*

Sources 2020;463:228191. DOI: 10.1016/j.jpowsour.2020.228191.

2. Huang ZJ, Zhang C, Lv W et al. Realizing stable lithium deposition by in situ grown Cu_2S nanowires inside commercial Cu foam for lithium metal anodes. *J Mater Chem A* 2019;7:727–732. DOI: 10.1039/c8ta10341k.

3. Wang Z, Cheng D, He H, Zhou K. Hierarchical nanosheet arrays of metal oxides guide uniform deposition for lithium anodes. *ACS Sustainable Chem Eng* 2020;8:102–110. DOI: 10.1021/acssuschemeng.9b04416.

4. Zhu JF, Chen J, Luo Y et al. Lithiophilic metallic nitrides modified nickel foam by plasma for stable lithium metal anode. *Energy Storage Mater* 2019;23:539–546. DOI: 10.1016/j.ensm.2019.04.005.

5. Lei MN, Wang JG, Ren LB et al. Highly lithiophilic cobalt nitride nanobrush as a stable host for high-performance lithium metal anodes. *ACS Appl Mater Interfaces* 2019;11:30992–30998. DOI: 10.1021/acsami.9b09975.

6. Lu WY, Wu C, Wei WF, Ma JM, Chen LB, Chen YJ. Lithiophilic NiO hexagonal plates decorated Ni collector guiding uniform lithium plating for stable lithium metal anode. *J Mater Chem A* 2019;7:24262–24270. DOI: 10.1039/c9ta09396f.

7. Huang X, Feng XY, Zhang B et al. Lithiated $NiCo_2O_4$ nanorods anchored on 3D nickel foam enable homogeneous Li plating/stripping for high-power dendrite-free lithium metal anode. *ACS Appl Mater Interfaces* 2019;11:31824–31831. DOI: 10.1021/acsami.9b08438.

8. Huang GX, Chen SR, Guo PM. In situ constructing lithiophilic NiF_x nanosheets on Ni foam current collector for stable lithium metal anode via a succinct fluorination strategy. *Chem Eng J* 2020;95:125122. DOI: 10.1016/j.cej.2020.125122.

9. Zhao Y,. Hao SG, Su L, Ma ZP, Shao GJ. Hierarchical Cu fibers induced Li uniform nucleation for dendrite-free lithium metal anode. *Chem Eng J* 2020;392:123691. DOI: 10.1016/j.cej.2019.123691.

10. Zhang Z, Wang JL, Yan XF et al. In-situ growth of hierarchical N-doped CNTs/Ni Foam scaffold for dendrite-free lithium metal anode. *Energy Storage Mater* 2020;29:332–340. DOI: 10.1016/j.ensm.2020.04.022.

11. Wu SL, Zhang ZY, Lan MH et al. Lithiophilic Cu-CuO-Ni hybrid structure: Advanced current collectors toward stable lithium metal anodes. *Adv Mater* 2018;30:1705830. DOI: 10.1002/adma.201705830.

12. Zhu WH, Deng W, Zhao F, Liang SS, Zhou XF, Liu ZP. Graphene network nested

Cu foam for reducing size of lithium metal towards stable metallic lithium anode. *Energy Storage Mater* 2019;21:107–114. DOI: 10.1016/j.ensm.2018.12.001.

13. Wei L, Li L, Zhao T et al. MOF-derived lithiophilic CuO nanorod arrays for stable lithium metal anodes. *Nanoscale* 2020;12:9416–9422. DOI: 10.1039/d0nr01091j.

14. Zhang C, Lv W, Zhou GM et al. Vertically aligned lithiophilic CuO nanosheets on a Cu collector to stabilize lithium deposition for lithium metal batteries. *Adv Energy Mater* 2018;8:1703404. DOI: 10.1002/aenm.201703404.

15. Zhang R, Wen SW, Wang N et al. N-doped graphene modified 3D porous Cu current collector toward microscale homogeneous Li deposition for Li metal anodes. *Adv Energy Mater* 2018;8:1800914. DOI: 10.1002/aenm.201800914.

16. Luan JY, Zhang Q, Yuan HY et al. Plasma-strengthened lithiophilicity of copper oxide nanosheet-decorated Cu foil for stable lithium metal anode. *Adv Sci* 2019;6: 1901433. DOI: 10.1002/advs.201901433.

17. Wang SH, Yin YX, Zuo TT et al. Stable Li metal anodes via regulating lithium plating/stripping in vertically aligned microchannels. *Adv Mater* 2017;29:1703729. DOI: 10.1002/adma.201703729.